Stereo Viewing 3-Component, Planar PIV Utilizing Fuzzy Inference

Mark P. Wernet
Lewis Research Center
Cleveland, Ohio

National Aeronautics and
Space Administration

STEREO VIEWING 3-COMPONENT, PLANAR PIV
UTILIZING FUZZY INFERENCE

Mark P. Wernet
National Aeronautics and Space Administration
Lewis Research Center
Cleveland, Ohio

ABSTRACT

An all electronic 3-D Digital Particle Image Velocimetry (DPIV) system has been developed for use in high velocity (supersonic) flows. Two high resolution CCD cameras mounted in a stereo viewing configuration are used to determine the out-of-plane velocity component from the difference of the in-plane velocity measurements. Double exposure image frames are acquired and Fuzzy inference techniques are used to maximize the validity of the velocity estimates obtained from the auto-correlation analysis. The CCD cameras are tilted relative to their respective lens axes to satisfy Scheimpflug's condition. Tilting the camera film plane ensures that the entire image plane is in focus. Perspective distortion still results, but can be corrected by proper calibration of the optical system. A calibration fixture is used to determine the experimental setup parameters and to assess the accuracy to which the z-plane displacements can be estimated. The details of the calibration fixture and procedure are discussed in the text. A pair of pulsed Nd:YAG lasers operating at 532 nm are used to illuminate the seeded flow from a convergent nozzle operated in an underexpanded condition. The light sheet was oriented perpendicular to the nozzle flow, yielding planar cross-sections of the 3-component velocity field at several axial stations. The key features of the supersonic jet are readily observed in the cross-plane vector plots.

INTRODUCTION

PIV is a widely used technique for measuring the in-plane two-component velocity field across a planar region of a flow field illuminated by a pulsed laser light sheet. Particles entrained in the fluid scatter light which is collected normal to the plane of the light sheet. The collected light is imaged onto a photographic plate or a CCD camera. Multiple images of the particles are recorded via short time intervals between laser light sheet pulses. The exposures may be recorded either on a single photographic plate or on a CCD image frame. When CCD cameras are used to record the collected light, single exposures may also be recorded on separate image frames enabling more flexibility in the subsequent data processing.

Multiple image frame recording can be processed via either cross-correlation, particle tracking or a combination of both techniques depending on the seed particle density. For high seed density flows correlation techniques are typically employed where the average velocity across a small subregion is computed.[1,2] This process is repeated over a regular grid across the image frame yielding the velocity vector map. In low seed density cases, particle tracking techniques are employed to determine the velocity of individual particles on the image frame.[3,4] In some instances, both techniques can be used to improve on the spatial resolution of the resulting velocity vector map.[5,6]

In cases with multiple exposures recorded on a single image frame the data processing must be done using an auto-correlation technique. Again the average velocities across small sub-regions of the flow are determined over a regular grid. The auto-correlation operation places certain restrictions on the minimum displacement of the recorded particle images between exposures, therefore reducing the dynamic range.[1]

Although PIV has made 2-component planar measurements rather commonplace, many fluid engineering problems of interest are fully three dimensional and therefore do not possess a plane of symmetry for easy 2-component, planar measurements. Many approaches have been proposed and investigated for obtaining 3-component velocity information utilizing the PIV technique. These approaches can be broken into two separate classes: 3-component velocity measurements in a volume; and 3-component velocity measurements across a plane. Most of the volumetric approaches are limited to tracking a relatively low number of particles in the volume and suffer from particle overlap ambiguities.[7-9] Holographic techniques have also been proposed and demonstrated for volume 3-component velocity estimates via particle tracking.[10] Barnhart, Adrian ,et. al. have demonstrated a holographic PIV system employing high seed particle density and correlation data reduction.[11]

The 3-component planar measurement region techniques are simply an extension of the in-plane 2-component PIV technique. In the planar approach, multiple recording cameras in a stereo viewing configuration or creative techniques for combining multiple views on a single camera are used.[12-14] There are two primary configurations for stereo PIV: lens translation; and angular displacement, as shown in figure 1a and b. Lens translation is simple and for small field angles results in no appreciable optical distortion, but the common image area from the two cameras may be restrictively small unless the field angles are enlarged.[13,15,16] The use of large field angles in the displacement technique increases the sensitivity to the out-of-plane displacement, but will also produce perspective distortion in the image.[17]

The angular displacement technique is considered to be more accurate; however, this technique results in perspective distortion on the image plane and typically requires a large depth of field to avoid defocusing across the image plane.[10,13] The image plane of best focus does not fall on the straight back camera film plane, resulting in blurring at the edges of the image, see figure 1b. The use of high f/number collection optics increases the depth of field and minimizes the blurring. The errors of perspective distortion can be ignored by keeping the coupling angle between the cameras small. However, sensitivity to the out-of-plane component is then reduced.[18,19] A back reflection technique has also been proposed to completely remove the perspective distortion.[10]

The large depth of field requirement of the angular displacement technique is easily eliminated by tilting the film plane such that the Scheimpflug condition is satisfied.[10,17,20] The Scheimpflug condition requires that the image plane, object plane and the median plane through the lens all intersect at a common point, see figure 2. The tilted object plane is imaged onto a tilted image plane where all points are in focus and the depth of field requirements of the optical system are reduced. The object to image distances vary horizontally across the image, resulting in perspective distortion. Both the vertical and horizontal magnification vary as a function of horizontal position on the image plane. The resulting two camera views of a rectangular object are shown in figure 2. These distortions can be accounted for in the data processing. The advantages of the angular displacement technique are the large field of view and the improved accuracy in estimating the out-of-plane displacement. An indirect advantage of the stereo viewing configuration is the collection of the particulate scattered light from an angle other than 90° from the

scattering plane. The scattering efficiency reaches a minimum at 90° collection for the case of p-polarized light and small (~1µm) particles, therefore, the oblique collection angles collect more light than would be detected from a standard PIV setup.

In this work we will describe and demonstrate an angular displacement, stereo viewing, tilt-back camera optical system satisfying the Scheimpflug condition. The equations relating object to image space are derived and used to perform an error analysis on the performance of the technique. The calibration equipment and procedure will be described. A set of validation tests are performed to verify the accuracy of the displacement estimates. Auto-correlation PIV data reduction is used to process the acquired images and Fuzzy inference techniques are used to improve the quality of the processed velocity vector maps.[21] Erroneous velocity vectors are corrected by using the Fuzzy inference engine to examine the secondary and lower amplitude peaks in the correlation plane and replace the erroneous vector with the correct velocity vector based on information from the surrounding velocity vectors. In this manner the correlation plane peak detection is treated as a pseudo particle tracking process where all of the peaks in the correlation plane are treated as candidate displacement peaks. Flow continuity rules govern the Fuzzy inference engine to correctly identify the true correlation displacement peak. An automatic thresholding operation is also demonstrated on the processed data to maximize the data quality. Finally, the system will be used to map a supersonic flow from an underexpanded jet using cross-plane slices through the jet flow. The system is shown to perform well even in the presence of the large velocity gradient caused by the Mach disk in the underexpanded flow.

OPTICAL SYSTEM

An all electronic 3-component PIV system was required to satisfy the needs of expedient processing and convenient storage of the velocity data. Although high resolution CCDs (1320×1040) were to be used, the resultant field of view is still quite small when compared to that available from photographic plates. Therefore, the angular displacement method was selected for the optical configuration so as to maximize the field of view. The two drawbacks of the angular displacement technique are that a large depth of field is required to keep the object plane in focus and the image magnification varies with horizontal position on the image plane. The resulting image of a rectangular

object is an isosceles trapezoid, see figure 2. By invoking the Scheimpflug condition, a technique commonly used in photography for image rectification, the large depth of field requirement is eliminated. The tilted object plane is exactly imaged onto the tilted image plane. Perspective distortion still remains in the image.

The amount of film plane tilt required varies depending on the object (d_o) and image (d_i) distances and the angular displacement half angle β. The total coupling angle between the cameras is 2β. The film plane tilt angle α is given by:

$$\alpha = \tan^{-1}\left[\frac{d_i \tan \beta}{d_o}\right] \quad (1)$$

The transformation from object to image space can be readily developed by invoking the colinearity condition which requires that a ray connecting an object (x_o,y_o) and image point (x_i,y_i) passes through the center of the lens as shown in figure 2. The object space coordinate system is centered at the intersection point of the two optical systems at the $z_o=0$ plane. The y-direction is out of the plane of the paper. Each camera film plane has a coordinate system centered about the middle of the film plane at (x_{fp_j}, y_{fp_j}). Again on the film plane the y-coordinate is out of the plane of the page and x lies in the plane. The resulting transformations for each camera view are:

$$x_{i_j} = \frac{d_{i_j}\left(x_o \cos \beta_j \pm z_o \sin \beta_j\right)}{\left\{d_{o_j} - (z_o \cos \beta_j \mp x_o \sin \beta_j) \pm \tan \alpha_j \left[x_o \cos \beta_j \pm z_o \sin \beta_j\right]\right\}} + x_{fp_j} \quad (2)$$

$$y_{i_j} = \frac{d_{i_j} y_o}{\left\{d_{o_j} - (z_o \cos \beta_j \mp x_o \sin \beta_j) \pm \tan \alpha_j \left[x_o \cos \beta_j \pm z_o \sin \beta_j\right]\right\}} + y_{fp_j} \quad (3)$$

where $j=1,2$ corresponds to the two camera views, and the top symbol in the $\pm$ corresponds to view #1 and the bottom symbol to view #2. A more useful form of the equations would be to express the object plane displacements in terms of the two measured image plane displacements (one set from each camera). The next few steps are designed to achieve the desired result. If we assume the particle moves to the new object plane location x_o+dx, y_o+dy, z_o+dz then on the image plane we can write for camera #1:

$$x_{i_1} = \frac{d_{i_1}\left[x_o \cos \beta_1 + z_o \sin \beta_1\right]}{d_{o_1} - z_o A_1 + x_o C_1} + x_{fp_1} \quad (4)$$

$$x_{i_1} + dx_{i_1} = \frac{d_{i_1}\left[(x_o + dx)\cos \beta_1 + (z_o + dz)\sin \beta_1\right]}{d_{o_1} - (z_o + dz)A_1 + (x_o + dx)C_1} + x_{fp_1} \quad (5)$$

where $C_1 = \sin \beta_1 + \tan \alpha_1 \cos \beta_1$,
$A_1 = \cos \beta_1 - \tan \alpha_1 \sin \beta_1$ and
dx_{ij} is the perceived displacement on the camera sensor surface.

Now by subtracting equation 4 from equation 5 and assuming terms of order dz^2, dx^2, $dzdx \ll d_{o_j}$ we find:

$$dx_{i_1} = M_1\left\{dx \cos \beta_1\left[1 - \left(x_o + z_o \tan \beta_1\right)\frac{M_1 C_1}{d_{i_1}}\right] + \right.$$
$$\left. dz \sin \beta_1\left[1 + \left(z_o + \frac{x_o}{\tan \beta_1}\right)\frac{M_1 A_1}{d_{i_1}}\right]\right\} \quad (6)$$

$$dy_{i_1} = M_1\left\{dy + dz \cdot y_o \frac{M_1 A_1}{d_{i_1}} - dx \cdot y_o \frac{M_1 C_1}{d_{i_1}}\right\} \quad (7)$$

and similarly for camera 2:

$$dx_{i_2} = M_2\left\{dx \cos \beta_2\left[1 + \left(x_o - z_o \tan \beta_2\right)\frac{M_2 C_2}{d_{i_2}}\right] - \right.$$
$$\left. dz \sin \beta_2\left[1 + \left(z_o - \frac{x_o}{\tan \beta_2}\right)\frac{M_2 A_2}{d_{i_2}}\right]\right\} \quad (8)$$

$$dy_{i_2} = M_2\left\{dy + dz \cdot y_o \frac{M_2 A_2}{d_{i_2}} + dx \cdot y_o \frac{M_2 C_2}{d_{i_2}}\right\} \quad (9)$$

where $C_2 = \sin \beta_2 + \tan \alpha_2 \cos \beta_2$,
$A_2 = \cos \beta_2 - \tan \alpha_2 \sin \beta_2$, and the optical system magnifications are:

$$M_1 = \frac{d_{i_1}}{d_{o_1} - z_o A_1 + x_o C_1}$$

and

$$M_2 = \frac{d_{i_2}}{d_{o_2} - z_o A_2 - x_o C_2}.$$

3

These equations describing the recorded particle displacements on the image planes can be inverted to get the explicit expressions describing the particle displacements in the vicinity of the object plane Δx, Δy, Δz:

$$\Delta z = \frac{\dfrac{dx_1}{M_1} - \dfrac{dx_2}{M_2}\gamma}{\sin\beta_1\left[1+\left(z_o+\dfrac{x_o}{\tan\beta_1}\right)\dfrac{M_1 A_1}{d_{i_1}}\right] + \sin\beta_2\left[1+\left(z_o-\dfrac{x_o}{\tan\beta_2}\right)\dfrac{M_2 A_2}{d_{i_2}}\right]\gamma} \quad (10)$$

$$\Delta x = \frac{\dfrac{dx_2}{M_2} + \Delta z\sin\beta_2\left[1+\left(z_o-\dfrac{x_o}{\tan\beta_2}\right)\dfrac{M_2 A_2}{d_{i_2}}\right]}{\cos\beta_2\left[1+\left(x_o-z_o\tan\beta_2\right)\dfrac{M_2 C_2}{d_{i_2}}\right]} \quad (11)$$

$$\Delta y = \frac{dy_1}{M_1} - \Delta z\cdot y_o\frac{M_1 A_1}{d_{i_1}} + \Delta x\cdot y_o\frac{M_1 C_1}{d_{i_1}} \quad (12)$$

where:

$$\gamma = \frac{\cos\beta_1\left[1-\left(x_o+z_o\tan\beta_1\right)\dfrac{M_1 C_1}{d_{i_1}}\right]}{\cos\beta_2\left[1+\left(x_o-z_o\tan\beta_2\right)\dfrac{M_2 C_2}{d_{i_2}}\right]}$$

These equations describe the actual particle displacements in the vicinity of the object plane in terms of the measured displacements on the tilted CCD sensor surfaces in cameras 1 and 2 and the location of the particle in the object space. Equations 2 and 3 above can also be inverted so that the two stereo camera image coordinates (x_{i_j}, y_{i_j}) $(j=1,2)$ of a selected object plane point (x_o, y_o, z_o) can be calculated.

ERROR ANALYSIS

The equations above describing the physical particle displacements in terms of the two in-plane PIV displacements can be used to determine the errors in the measured velocity components. The computed displacements depend on many physical parameters in the optical setup which will be ignored in the analysis, since their values can be determined to reasonable accuracy and their effect should be minimal. Assuming that both optical systems are identical ($\beta_1=\beta_2$, $\alpha_1=\alpha_2$,

and d_i and d_o from both camera views are identical) the errors in Δz, Δx and Δy are given below:

$$\sigma_{\Delta z}^2 = \frac{\delta_{dx_1}^2}{\left[M_1\sin\beta\left\{\left[1+\left(z_o+\dfrac{x_o}{\tan\beta}\right)\dfrac{M_1 A}{d_i}\right]+\left[1+\left(z_o-\dfrac{x_o}{\tan\beta}\right)\dfrac{M_2 A}{d_i}\right]\gamma\right\}\right]^2} +$$

$$\frac{\delta_{dx_2}^2\gamma^2}{\left[M_2\sin\beta\left\{\left[1+\left(z_o+\dfrac{x_o}{\tan\beta}\right)\dfrac{M_1 A}{d_i}\right]+\left[1+\left(z_o-\dfrac{x_o}{\tan\beta}\right)\dfrac{M_2 A}{d_i}\right]\gamma\right\}\right]^2} + \quad (13)$$

$$\left[\delta_x\frac{\partial\Delta z}{\partial x}\right]^2 + \left[\delta_z\frac{\partial\Delta z}{\partial z}\right]^2$$

$$\sigma_{\Delta x}^2 = \frac{\delta_{dx_1}^2}{\left\{M_1\cos\beta\left[1-\left(x_o+z_o\tan\beta\right)\dfrac{M_1 C}{d_i}\right]\right\}^2} +$$

$$\left[\frac{-\tan\beta\left[1+\left(z_o+\dfrac{x_o}{\tan\beta}\right)\dfrac{M_1 A}{d_i}\right]\sigma_{\Delta z}}{\left[1-\left(x_o+z_o\tan\beta\right)\dfrac{M_1 C}{d_i}\right]}\right]^2 + \quad (14)$$

$$\left[\delta_x\frac{\partial\Delta x}{\partial x}\right]^2 + \left[\delta_z\frac{\partial\Delta x}{\partial z}\right]^2$$

$$\sigma_{\Delta y}^2 = \delta_y^2\left[\Delta x\frac{M_1 C}{d_i} - \Delta z\frac{M_1 A}{d_i}\right]^2 + \left[\frac{\delta_{dy_1}}{M_1}\right]^2 +$$

$$\left[\sigma_{\Delta x}y_o\frac{M_1 C}{d_i}\right]^2 + \left[\sigma_{\Delta z}y_o\frac{M_1 A}{d_i}\right]^2 \quad (15)$$

where δ_{dx1}, δ_{dx2}, δ_{dy1} are the errors in determining the correlation peak locations, and δ_x, δ_y, δ_z are the errors in the location of the correlation subregion on the object plane. Some of the partial derivatives have not been explicitly shown due to their unruly size. The errors for Δx, Δy and Δz are plotted in figure 3 over a range of coupling half angles β for the case $y_o=0$ and $z_o=0$. The independent variable is x_o. The errors in determining the correlation peak location were assumed to be $\delta_{dxj}=\delta_{dyj}=0.05\varepsilon_p/M_j$, where ε_p is the camera pixel size.

4

Recall that the magnification is not constant in the image, hence the error will in general be a function of x_o and z_o. Two estimates of Δx and Δy are available, one from each camera view. Only one of the two expressions for the error in Δx and Δy have been included above. In the computations of Δx and Δy the average of the two estimates from each camera view will be used.

Figure 3a shows that the error in Δx changes very little with horizontal position, growing larger at the boundaries of the image and reaching a minimum at the center of the image. As the error coupling half-angle β is increased, the error in Δx increases. Figure 3b shows the error in Δy, which is relatively insensitive to horizontal position on the object plane and the coupling half angle. Increasing the coupling half angle causes an increase in the error of Δy only at the boundaries of the image. The errors remain relatively flat at the center of the image. Figure 3c shows the opposite trends from the previous two plots. Increasing the coupling half angle β decreases the out-of-plane displacement error in $\sigma_{\Delta z}$. The error in Δz is relatively insensitive to horizontal position on the image.

The major variables affecting the out-of-plane displacement Δz in equation 10 above can be determined by making some further simplifying assumptions. In addition to the assumptions made above we can also assume that $\delta_{dx_1} = \delta_{dx_2}$ and $x_o=0$ then:

$$\sigma_{\Delta z} = \frac{\delta_{dx}}{\sqrt{2}M\sin\beta} \qquad (16)$$

where $M=d_i/d_o$. Hence, we obtain the obvious result that the error in the out-of-plane displacement is directly related to the error in estimating the correlation peak location on the CCD sensor and inversely related to the product of the sine of the optical system coupling half angle and the optical system magnification. Simplifying equation 11 in a similar form and combining with equation 16 we find:

$$\sigma_{\Delta z} = \frac{\sigma_{\Delta x}}{\tan\beta} \qquad (17)$$

This simplification allows us to define an approximate ratio of the error in Δz to the error in Δx. For the case where $\beta=30°$, the error in Δz is 1.7 times as large as the in-plane error $\sigma_{\Delta x}$. At the limit of $\beta=45°$, the error in the out-of-plane displacement equals the in-plane displacement error.

In the preceding analysis we assumed that there was no limitation on the minimum displacement that could be detected by each of the stereo viewing cameras. In reality only the cross-correlation technique possesses this property. Auto-correlation requires that the particles displace by at least their diameters so that the displacement peak can be distinguished from the zero-order peak. If the flow velocity vector happens to point directly along the optical axis of one of the cameras, the auto-correlation technique will yield a "dead-band" region where particle displacements can not be detected. The "dead-band" feature of the auto-correlation technique has been ignored in the error analysis. The experiments below were designed so that the auto-correlation analysis would detect measurable displacements.

CALIBRATION SYSTEM/OPTICAL HARDWARE

The optical system is shown in figure 4. The cameras are mounted on carts with sliding dogs that fit into concentric radius grooves in the mounting table. The center location of the radial grooves is located 8 inches from the edge of the table. This configuration permits easy changes in the optical system coupling angle while maintaining a common focal point between the cameras. The lenses are mounted directly on the sliding carts and are directed normal to the radial grooves in the table. The cameras bodies are mounted independent of the lens on the sliding carts and are on rotatable bases so that the proper tilt angle α can be introduced. A flexible baffle is placed between the lens and the camera to prevent stray light from reaching the CCD sensor.

A calibration target consisting of an optical flat with a reticle grid on the front surface is mounted in a jig that connects to the camera mounting table to hold the target at center of rotation of the optical system. The reticle grid contains 5 horizontal and 5 vertical lines on 5 mm centers. The reticle is mounted on a 2-axis micrometer stage on the calibration jig support. The stages allow the calibration target to be moved to multiple object z_o-planes.

The optical system is setup so that the middle vertical and horizontal lines on the reticle are at the center of the camera system field of view. The images from the two cameras are electronically subtracted to aid in fine tuning the alignment. The center vertical and horizontal lines are made to overlap as best as possible with the

calibration target at the z_o=0 plane. Calibration data are then taken at multiple z_o-planes (0, ±0.5, ±1 mm).

The calibration images are processed and used to determine the overall optical system setup parameters. The images are first processed using edge detection filters to find the horizontal and vertical lines on the ruled grid. The slopes and intercepts of all the lines (horizontal and vertical) are then determined in a global fitting operation. Knowledge about the vertical lines being parallel to each other and also perpendicular to the center horizontal line are incorporated into the fitting procedure. The slope of the center horizontal line is used to determine and later correct for the amount of rotation in each camera image about the optical axis. The extrapolated horizontal lines intersect at a point in space which is used to define a keystone transformation back to a Cartesian object space using just the slopes of either the top or bottom horizontal lines.[22] The simple geometric keystone transformation is used to determine the optical system magnification at the center of the object plane x_o=0, y_o=0, z_o=0.

The intersection points of all of the lines in the calibration target for each camera view at all of the z_o-planes are then used along with the optical system magnification (for each view) to fit for the other optical system parameters: $\alpha, \beta, d_{i_j}, d_{o_j}$, and the center coordinates of the object space on the CCD sensor plane x_{fp_j}, y_{fp_j}. A function minimization procedure is used to minimize the distances between the reconstructed object plane coordinates of the intersecting lines on the calibration target at the multiple z-planes and the known 3-D coordinates of the intersecting lines on calibration target at the mechanically displaced z-plane locations. The fit parameters constitute the stereo view optical system calibration allowing for the transformation from image to object space, or vice versa.

EQUIPMENT AND DATA PROCESSING

A pair of Nd:YAG lasers with 200 mJ/pulse energy at 532nm are used to provide light sheet illumination. Two Kodak Megaplus 1.4 cameras are connected to EPIX framegrabber boards for data acquisition into a single PC. The camera resolution is 1320×1040 and the pixels are 6.8μm square with a 100% fill factor. Double exposure images are acquired with the illumination/recording system. The acquired image frames are processed via auto-correlation and a Fuzzy logic correlation peak detection algorithm is employed.

The image frames acquired with the angular displacement optical viewing system contain perspective distortion where a rectangular object becomes an isosceles trapezoid. The perspective distortion has two main components: an anamorphic component; and a shearing component. Anamorphic distortion manifests itself in a foreshortening of the x-dimension by approximately the cosine of the object plane tilt angle. The shearing distortion is caused by the variation in the y-plane magnification with horizontal position. The shear is largest at the upper and lower boundaries of the image and smallest along the horizontal centerline. In order to obtain a regular grid of velocity measurements on the object plane, the location and spacing of the image plane correlation subregions must vary with position. A regular grid of points is defined on the object plane and the corresponding set of image plane points for each camera view is computed and used to determine the center location of the correlation subregions. The computed velocity vectors are distorted by an amount dependent on their position on the image frame. On average, the anamorphic distortion for the 30° viewing angle is approximately 15%, while the shear is approximately 3%. For small subregion sizes, the local distortion remains relatively constant across the subregion. The distortion is acceptable if it is constant across the subregion since the distortion is removed when the displacement vectors are mapped back to the object plane in the 3-D reconstruction process. Also, the 3-D reconstruction is initiated by constructing a planar grid in the object space from which the correlation subregion center locations are computed for each camera view. The average displacements across the subregions are computed and used to determine the out-of-plane displacements. Hence, the reconstruction does not rely on accurately matching the object plane coordinates of two image plane points (i.e. particle images) to estimate the out-of-plane displacement. Rather the out-of-plane displacement is computed from the difference of the average in-plane displacement over an extended subregion in each camera view, which is only sensitive to the order of the size of the subregion.

During the course of the auto-correlation data reduction software development, the choice of the image threshold level applied prior to auto-correlation processing was found to significantly affect the quality of the resulting vector map. The threshold level affects the amplitude and width of the zero-correlation peak and hence affects the ability of the correlation peak detection software to discern the first order particle displacement peak from the zero order peak. The variation in particulate seed across the image resulted in

widely varying background noise levels. A high threshold level may produce good results in a high noise area, but will yield no correlation results in low noise regions of the image. An automatic threshold algorithm was found to yield good results over both high and low noise regions of the image. The auto-threshold technique simply computes the ratio of the number of non-zero pixels to the total number of pixels in each subregion. The threshold level is continuously increased until a ratio of 5% is achieved. The auto-correlation operation is then performed on the thresholded subregion.

The velocity vector map obtained using auto-correlation processing typically results in a few erroneous vectors in the velocity vector map. Many factors influence the ability of the data reduction software to accurately detect the true secondary peak corresponding to the average particle displacement across the subregion.[6] For each subregion processed, the five largest peaks (other than the zero-order peak) on the correlation plane are detected and stored. After all of the subregions have been processed the Fuzzy inference engine is applied. At each subregion a set of velocity vectors are detected, which are then examined to determine the most probable displacement vector for that subregion. The velocity vectors in the surrounding subregions are also used in the evaluation of the candidate list at a given grid point. In this manner the correlation plane peak detection is treated as a pseudo particle tracking process where all of the peaks in each subregion's correlation plane are treated as candidate displacement peaks. Flow continuity rules govern the Fuzzy inference engine to correctly identify the true correlation displacement peak.

VALIDATION TESTS

Tests were performed to validate the capability of the stereo view optical system to accurately reconstruct the recorded three-dimensional displacements. The goal of the tests were twofold: first to determine if the optical system calibration was accurate; and second to determine if there were any residual effects of the perspective distortion in the reconstructed object field. Rather than use a computer simulation which neglects the effects of optical noise, digitization error, and lens distortion, the tests were designed to use as much of the actual experimental hardware as was feasible. The camera system was configured with a coupling half angle $\beta=30°$. A card with a simulated field of randomly sized and spaced small white specks on a black background was mounted on the face of the calibration target reticle. The recorded images contain particles

that are up to 4×4 pixels in size and there are approximately 8 to 10 particles per 32×32 subregion. The simulated particle field could then be moved via the 2-axis translation stage so that the z_o and x_o positions of the simulated particle field could be altered between image recordings. The single exposure images were then electronically added to produce a double exposure image for each camera view.

The simulated particle field was moved through a variety of Δx and Δz displacements. The simulated double exposure images were then processed using the auto-correlation data processing software. The two velocity vector image maps obtained from the stereo views were then processed via the 3-D reconstruction software to compute the displacement field. Figure 5 shows the displacement field results from a particulate field mechanical displacement of (0.5, 0.0, 0.3 mm). The correlation subregions size was 64×64 with 50% overlap. The vector field plotted shows the Δx and Δy components of the displacement in the magnitude and angle of the vectors. The out-of-plane displacement Δz is encoded in the color of the displacement vectors. Some spurious vectors are observed in the displacement map which resulted from low particulate seeding in these areas. The averages of the measured displacements over the entire field are: Δx:0.493 ± 0.034 mm, Δy: 0.004 ± 0.011 mm, Δz:0.299 ± 0.059 mm. The absolute value of the Δy displacements were taken before computing the mean values to ensure that any symmetric distortions in the image did not cancel out. The results show that the measured displacements accurately reproduce the true mechanical displacement of the simulated particulate field. No residual effects from the image plane distortion are observed in the final reconstructed object plane. The subregion size used for this validation test are the largest that would be used to reduce the image frames, therefore, perspective distortion effects should be negligible. Computing the ratio of out-of-plane to in-plane errors yields $\sigma_{\Delta z}/\sigma_{\Delta x} = 1.7$, which agrees with the ratio predicted from the error analysis for an optical system coupling half angle of $\beta=30°$.

NOZZLE DATA

The stereo view PIV system was next used to measure the 3-component velocity field of a nozzle jet flow. The nozzle centerline was directed parallel to the bisector of the stereo cameras as shown in figure 6. This optical configuration allowed the measurement of cross sections of the nozzle flow at various downstream

7

locations. Again the camera half angle was set to β =30°. The Nd:YAG laser beam was formed into a 2×40 mm sheet, which was directed from above the nozzle to a beam trap below.

The nozzle consisted of a constant radius contraction with an exit diameter of 6.35 mm. The flow was seeded in the plenum section using a commercial six-jet atomizer filled with Rosco's smoke juice. The resulting mean seed particle size was approximately 1 μm. No ambient seed was introduced. The nozzle was operated at a plenum pressure of 75 psi, yielding an underexpanded supersonic flow.[6] The flow from this nozzle has previously been characterized and contains a Mach disk approximately 1.5 nozzle diameters downstream of the nozzle exit plane. The flow upstream of the nozzle is approximately 630 m/s and downstream of the Mach disk drops to 150 m/s. The flow then repeatedly ramps back up and shocks back down. Inter-frame exposure times from 0.8 to 1.2 microseconds were used to record the velocity field. The camera lenses were operated at f/10 and the object and image distances were 322 and 47 mm. The imaged area was approximately 60×40 mm.

Cross-plane measurements were obtained at five axial stations: 1.1, 1.6, 1.9, 2.6, and 3.0 nozzle diameters downstream. The images were processed with an auto-correlation subregion size of 32×32 with 50% overlap. Six exposure sets at each measurement station were acquired and the resulting velocity vector maps averaged. Figure 7 shows the resulting 3-component, planar cross sections of the measured nozzle flow, where the vector magnitudes are color coded. The vector plot at z/d=1.1 shows the supersonic accelerating flow. The cross sections at z/d=1.6 and 1.9 show the decelerated flow and the presence of the Mach disk. The Mach disk is denoted by the low velocity core flow containing the light green/yellow velocity vectors which is surrounded by the higher velocity (blue coded) outer flow. At z/d=2.6 the flow has ramped back up to supersonic and become more turbulent. The final station at z/d=3.0 shows again a decelerated flow which is also more turbulent than the measurements obtained closer to the nozzle exit plane.

CONCLUSIONS

An all electronic, angular displacement, stereo viewing 3-component PIV system has been described and demonstrated. The image plane focus was optimized by employing the Scheimpflug condition via a tilted camera back. An error analysis showed the expected errors in each of the measured displacements as a function of horizontal position on the object plane. Residual perspective distortion from the oblique viewing direction was demonstrated to be negligible for small (32×32) correlation subregions. The out-of-plane displacement error was shown to be approximately 1.7 times larger than the in-plane error for an optical system coupling half angle of 30°. Fuzzy inference techniques were used to analyze the correlation plane results to optimize the validity of the velocity vector maps. The stereo view PIV system was demonstrated on an underexpanded supersonic nozzle flow, where the light sheet was perpendicular to the flow direction. The system was shown to be sensitive to the large velocity gradients in the nozzle flow.

REFERENCES

1) Adrian, R. J., "Multi-Point Optical Measurements of Simultaneous Vectors in Unsteady Flow - A Review", *Int. J. of Heat and Fluid Flow*, Vol 7, pp127-145, 1986.

2) Willert, C. E. and Gharib, M., "Three-Dimensional Particle Imaging With a Single Camera", *Experiments in Fluids*, 12, pp353-358, 1992.

3) Wernet, M. P. and Pline, A., "Particle Image Velocimetry for the Surface Tension Driven Convection Experiment Using a Particle Displacement Tracking Technique", *Fourth International Conference on Laser Anemometry*, Cleveland, OH, pp 315-325, August 5-9, 1991.

4) Wernet, M. P., "Particle Displacement Tracking Applied to Air Flows", *Fourth Inter-national Conference on Laser Anemometry*, Cleveland, OH, pp 327-335, August 5-9, 1991.

5) Keane, R. D., Adrian, R. J. and Zhang, Y., "Super-Resolution Particle Imaging Velocimetry", *Meas. Sci. Technol.*, 6, pp754-768, 1995.

6) Wernet, M. P., "Fuzzy Inference Enhanced Information Recovery from Digital PIV Using Cross-Correlation Combined with Particle Tracking", *SPIE Conference on Optical Diagnostics in Fluid and Thermal Flow*, Vol 2546, San Diego, CA, July 9-14, 1995.

7) Adamczyk, A. A., and Rimai, L., "Reconstruction of a 3-Dimensional Flow Field From Orthogonal

Views of Seed Track Video Images", *Experiments in Fluids*, **6**, pp380-386, 1988.

8) Kobayashi, T., Saga, T., Sekimoto, K., "Velocity Measurement of Three-Dimensional Flow Around Rotating Parallel Disks by Digital Image Processing", FED-Vol. 85, Flow Visualization, pp 29-36, December 10-15, 1989.

9) Okamoto, K., Hassan, Y. A., Schmidl, W. D., "Simple Calibration Technique Using Image Cross-Correlation For Three Dimensional PIV", FED-Vol. 209, Flow Visualization and Image Processing of Multiphase Systems, pp99-106, 1995.

10) Hinsch, K. D., "Three-Dimensional Particle Velocimetry", *Meas. Sci. Technol.*, **6**, pp742-753, 1995.

11) Barnhart, D. H., Adrian, R. J., Papen, G. C., "Phase-Conjugate Holographic System for High Resolution Particle Image Velocimetry", *Appl. Opt.*, Vol 33, No. 30, pp7159-7170, 1994.

12) Grant, I., Fu, S., Pan, X., Wang, X., "The Application of an In-Line, Stereoscopic, PIV System to 3-Component Velocity Measurements", *Experiments in Fluids*, **19**, pp214-221, 1995.

13) Gauthier, V. and Riethmuller, M. L., "Particle Image Velocimetry", von Karman Institute for Fluid Dynamics Lecture Series 1988-06, N89-17179, March 21-25, 1988.

14) Willert, C. E. and Gharib, M., "Digital Particle Image Velocimetry", *Experiments in Fluids*, **10**, pp181-193, 1991.

15) Prasad, A. K. and Adrian, R. J., "Stereoscopic Particle Image Velocimetry Applied to Liquid Flows", *Sixth International Symposium on Applications of Laser Techniques to Fluid Mechanics*, Lisbon, Portugal, July 20-23, pp6.1.1-6.1.8, 1992.

16) Arroyo, M. P. and Greated, C. A., "Stereoscopic Particle Image Velocimetry", *Meas. Sci. Technol.*, **2**, pp1181-1186, 1991.

17) Kingslake, R., *Optics in Photography*, SPIE Optical Engineering Press, 1992.

18) Funes-Gallanzi, M. and Bryanston-Cross, P. J., "Solid State Visualization of a Highly Three Dimensional Flow Using Stereoscopic Particle Image Velocimetry (3DPIV)", *SPIE Conference on Optical Diagnostics in Fluid and Thermal Flow*, Vol 2005, San Diego, CA, pp 360-369, July 14-16, 1993.

19) Westerweel, J. and Nieuwstadt, F. T. M., "Performance Tests on 3-Dimensional Velocity Measurements with a Two-Camera Digital Particle-Image Velocimeter", *Fourth International Conference on Laser Anemometry*, Cleveland, OH, pp349-355, August 5-9, 1991.

20) Stephany, J. F. and Haas, W. E., "Keystone Compensation for Image Storage Systems", *Appl. Optics*, Vol 15, No. 6, pp 1626-28, 1976.

21) Wernet, M. P., "Fuzzy Logic Particle-Tracking Velocimetry", *SPIE Conference on Optical Diagnostics in Fluid and Thermal Flow*, Vol 2005, San Diego, CA, pp701-708, July 14-16, 1993.

22) Buchele, D., "Analytical Correction of Keystone Distortion", ADF Memorandum Task Order 45-21, NASA Contract NAS3-25767, 1990.
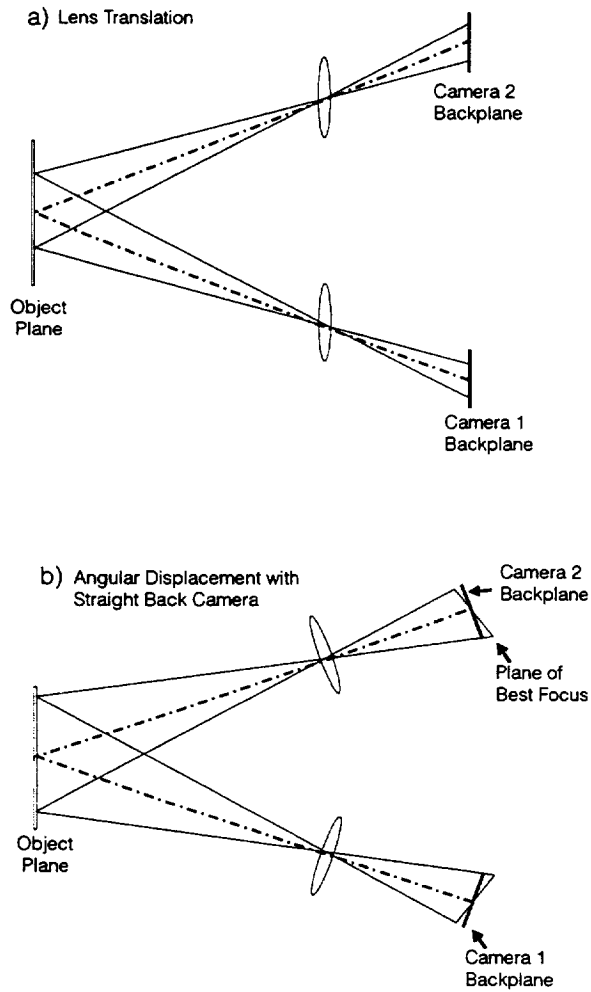
a) Lens Translation

Camera 2
Backplane

Object
Plane

Camera 1
Backplane

b) Angular Displacement with
Straight Back Camera

Camera 2
Backplane

Plane of
Best Focus

Object
Plane

Camera 1
Backplane

Scheimpflug
Condition

Image 2

α

β

d_i

Tilt-Back
Camera 2

Object
Plane

d_o

β

x_o, y_o

Object

Tilt-Back
Camera 1

x_i, y_i

y —→ z

x

Image 1

Figure 1: Schematic layouts of the two stereo view
optical configurations: a) lens translation; b)
angular displacement. The angular
displacement cameras are shown with straight
film backs. The plane of best focus does not
lie on the film plane.
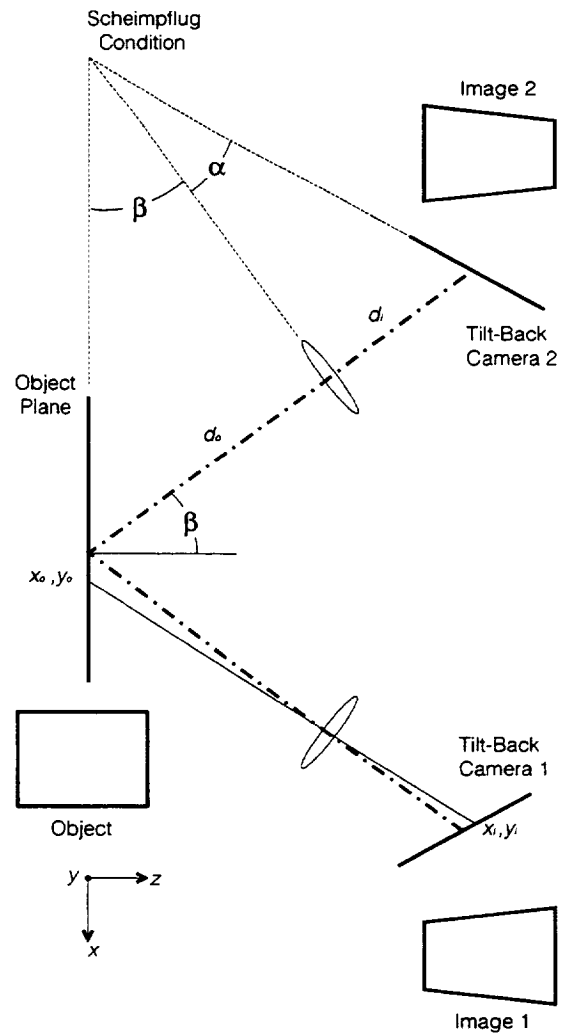
Figure 2:   Optical configuration satisfying
Scheimpflug's condition. The camera
backs are tilted by an amount α, and the
angular displacement half angle is β. A
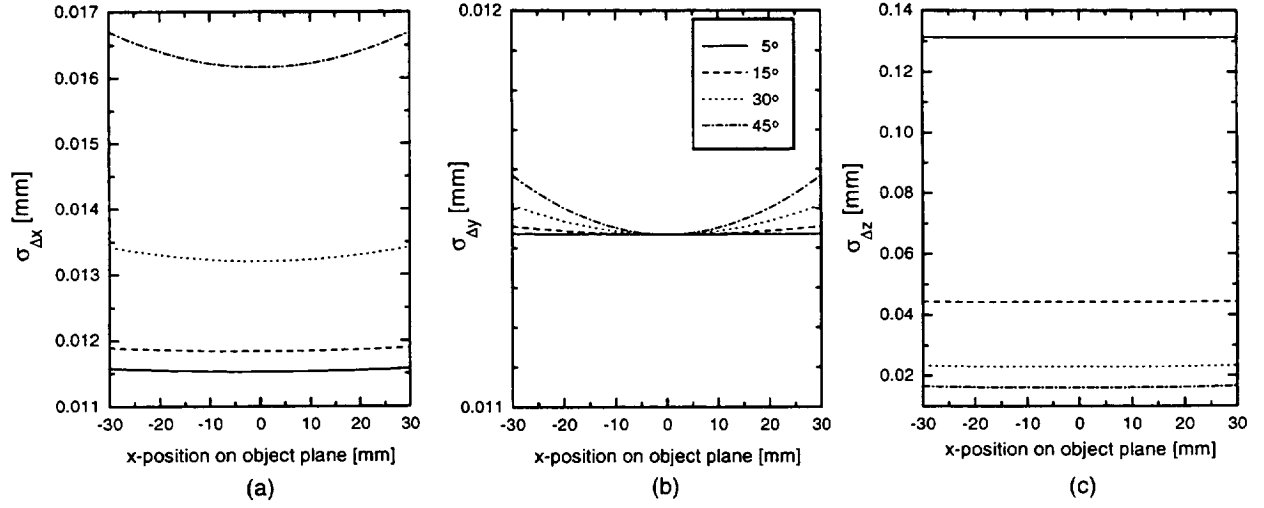rectangular object is shown to be imaged
into an isosceles trapezoid.

10

Figure 3: The error in Δx, Δy and Δz are plotted versus the horizontal position on the object plane. The errors are computed for a range of stereo camera coupling half angles (β=5°, 15°, 30°, 45°). The errors are only weak functions of horizontal position. The errors in Δx and Δz are strong functions of the optical system coupling half angle. The error in determining the correlation peak location on the CCD sensor was assumed to be $\delta_{dxj}=\delta_{dyj}=0.05\varepsilon_p/M_j$, where ε_p is the camera pixel size.
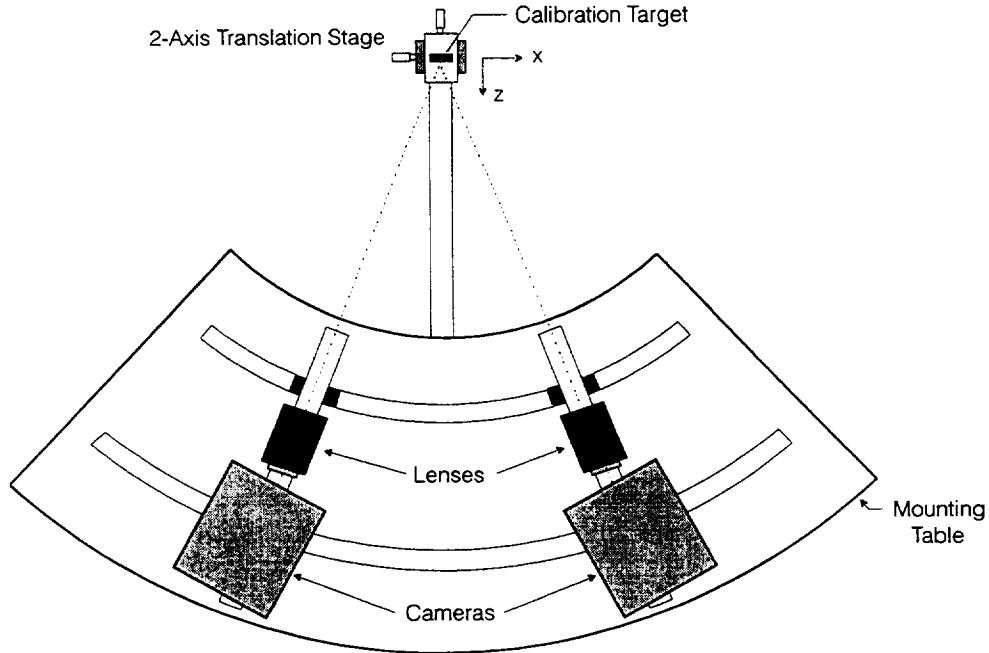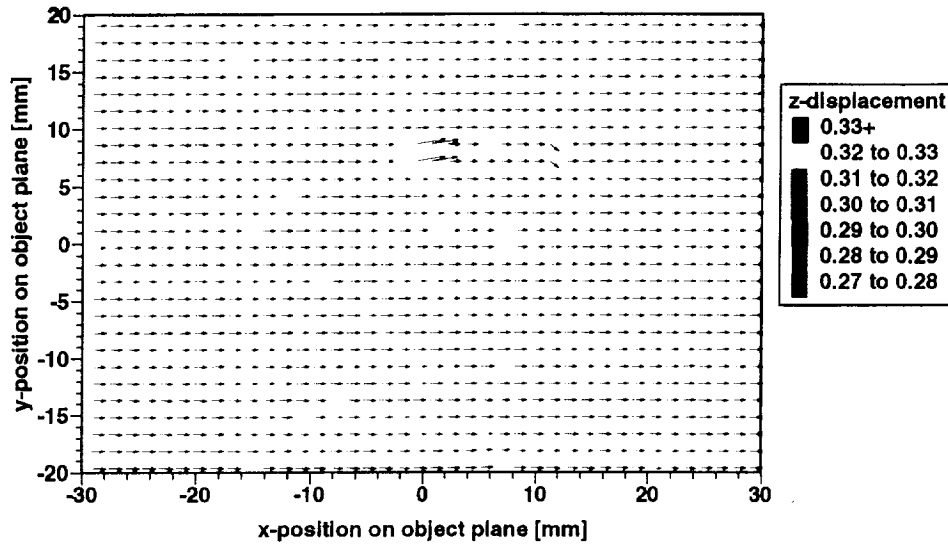

Figure 4: Orientation of optical hardware on the mounting table. The lens is mounted independent of the camera on sliding carts. The carts can be adjusted to change the coupling angle while maintaining a common focus point between the two cameras. The calibration target is shown on a two-axis translation stage.

11

Mechanical Displacements:	Measurements:
Δx: 0.5 mm	Δx: 0.493 ± 0.034 mm
Δy: 0.0 mm	Δy: 0.004 ± 0.011 mm
Δz: 0.3 mm	Δz: 0.299 ± 0.059 mm

Figure 5:   Validation test results for a mechanical translation of a simulated particle field. The in-plane displacements are depicted in the vector magnitude and angle. The out-of-plane displacements are encoded in the color of the vectors as shown by the accompanying key. The actual mechanical displacements and the average and standard deviation of the measured results across the plane are denoted in the figure. No residual effects from the perspective distortion are observed.
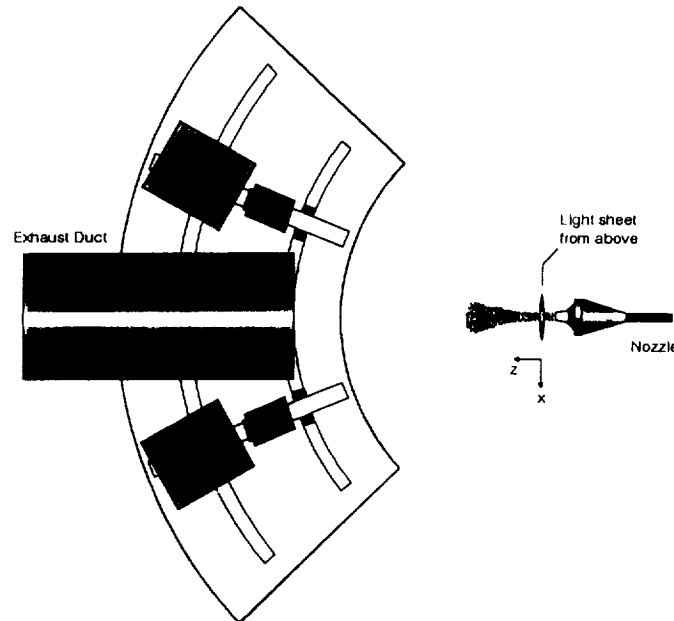

Figure 6:   Experimental setup for the nozzle flow measurements. The light sheet is directed from above to a beam dump below the nozzle. An exhaust duct is mounted between the cameras to collect the seeded air stream.

Velocity [m/s]
600+
500 to 600
400 to 500
300 to 400
200 to 300
100 to 200
0 to 100

z/d=1.1

z/d=1.6

z/d=1.9

z/d=2.6

z/d=3.0

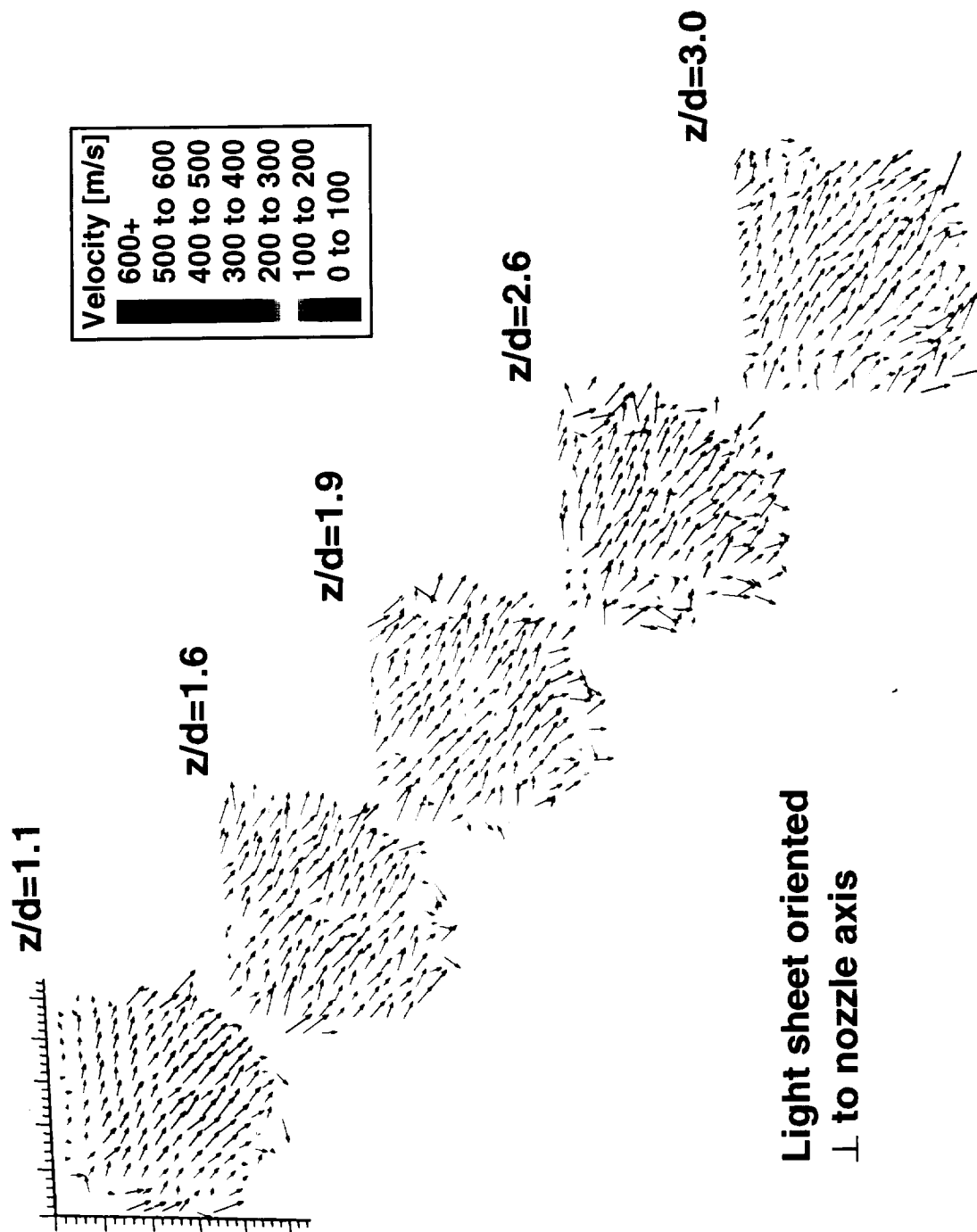Light sheet oriented ⊥ to nozzle axis

Figure 7: Cross-plane velocity vector plots at 5 axial stations. The development of the supersonic flow and the deceleration regions can be observed in the data. The flow becomes more turbulent as the axial position increases.

REPORT DOCUMENTATION PAGE

Public reporting burden for this collection of information is estimated to average 1 hour per response, including the time for reviewing instructions, searching existing data sources, gathering and maintaining the data needed, and completing and reviewing the collection of information. Send comments regarding this burden estimate or any other aspect of this collection of information, including suggestions for reducing this burden, to Washington Headquarters Services, Directorate for Information Operations and Reports, 1215 Jefferson Davis Highway, Suite 1204, Arlington, VA 22202-4302, and to the Office of Management and Budget, Paperwork Reduction Project (0704-0188), Washington, DC 20503.

1. AGENCY USE ONLY (Leave blank)	2. REPORT DATE	3. REPORT TYPE AND DATES COVERED
	June 1996	Technical Memorandum

4. TITLE AND SUBTITLE

Stereo Viewing 3-Component, Planar PIV Utilizing Fuzzy Inference

5. FUNDING NUMBERS

WU-505-62-50

6. AUTHOR(S)

Mark P. Wernet

7. PERFORMING ORGANIZATION NAME(S) AND ADDRESS(ES)

National Aeronautics and Space Administration
Lewis Research Center
Cleveland, Ohio 44135-3191

8. PERFORMING ORGANIZATION REPORT NUMBER

E-10278

9. SPONSORING/MONITORING AGENCY NAME(S) AND ADDRESS(ES)

National Aeronautics and Space Administration
Washington, D.C. 20546-0001

10. SPONSORING/MONITORING AGENCY REPORT NUMBER

NASA TM-107235
AIAA-96-2268

11. SUPPLEMENTARY NOTES

Prepared for the 19th Advanced Measurement and Ground Testing Technology Conference sponsored by the American Institute of Aeronautics and Astronautics, New Orleans, Louisiana, June 17-20, 1996. Responsible person, Mark P. Wernet, organization code 2520, (216) 433-3752.

12a. DISTRIBUTION/AVAILABILITY STATEMENT

Unclassified - Unlimited
Subject Category 35

This publication is available from the NASA Center for AeroSpace Information, (301) 621-0390.

12b. DISTRIBUTION CODE

13. ABSTRACT (Maximum 200 words)

An all electronic 3-D Digital Particle Image Velocimetry (DPIV) system has been developed for use in high velocity (supersonic) flows. Two high resolution CCD cameras mounted in a stereo viewing configuration are used to determine the out-of-plane velocity component from the difference of the in-plane velocity measurements. Double exposure image frames are acquired and Fuzzy inference techniques are used to maximize the validity of the velocity estimates obtained from the auto-correlation analysis. The CCD cameras are tilted relative to their respective lens axes to satisfy Scheimpflug's condition. Tilting the camera film plane ensures that the entire image plane is in focus. Perspective distortion still results, but can be corrected by proper calibration of the optical system. A calibration fixture is used to determine the experimental setup parameters and to assess the accuracy to which the z-plane displacements can be estimated. The details of the calibration fixture and procedure are discussed in the text. A pair of pulsed Nd:YAG lasers operating at 532 nm are used to illuminate the seeded flow from a convergent nozzle operated in an underexpanded condition. The light sheet was oriented perpendicular to the nozzle flow, yielding planar cross-sections of the 3-component velocity field at several axial stations. The key features of the supersonic jet are readily observed in the cross-plane vector plots.

14. SUBJECT TERMS

Particle tracking; Velocimetry

15. NUMBER OF PAGES

15

16. PRICE CODE

A03

17. SECURITY CLASSIFICATION OF REPORT	18. SECURITY CLASSIFICATION OF THIS PAGE	19. SECURITY CLASSIFICATION OF ABSTRACT	20. LIMITATION OF ABSTRACT
Unclassified	Unclassified	Unclassified	

NSN 7540-01-280-5500

National Aeronautics and
Space Administration

Lewis Research Center
21000 Brookpark Rd.
Cleveland, OH 44135-3191